

The Real-Time Distributed Control of the Virgo Interferometric Detector of Gravitational Waves

F. Acernese, P. Amico, M. Alshourbagy, F. Antonucci, S. Aoudia, P. Astone, S. Avino, D. Babusci, R. Barillé, G. Ballardin, F. Barone, L. Barsotti, M. Barsuglia, T. S. Bauer, F. Beauville, S. Bigotta, M. A. Bizouard, C. Boccara, F. Bondu, L. Bosi, C. Bradaschia, S. Birindelli, S. Braccini, J. F. J. van den Brand, A. Brillet, V. Brisson, D. Buskalic, E. Calloni, E. Campagna, F. Carbognani, F. Cavalier, R. Cavalieri, G. Cella, E. Cesarini, E. Chassande-Mottin, N. Christensen, A.-C. Clapson, F. Cleva, C. Corda, A. Corsi, F. Cottone, J.-P. Coulon, E. Cuoco, A. Dari, V. Dattilo, M. Davier, M. del Prete, R. De Rosa, L. Di Fiore, A. Di Virgilio, B. Dujardin, A. Eleuteri, M. Evans, I. Ferrante, F. Fidecaro, I. Fiori, R. Flaminio, J.-D. Fournier, S. Frasca, F. Frasconi, A. Freise, L. Gammaitoni, F. Garufi, E. Genin, A. Gennai, A. Giazotto, G. Giordano, L. Giordano, R. Gouaty, D. Grosjean, G. Guidi, S. Hamdani, S. Hebri, H. Heitmann, P. Hello, D. Huet, S. Karkar, S. Kreckelbergh, P. La Penna, M. Laval, N. Leroy, N. Letendre, B. Lopez, M. Lorenzini, V. Lorette, G. Losurdo, J.-M. Mackowski, E. Majorana, C. N. Man, M. Mantovani, F. Marchesoni, F. Marion, J. Marque, F. Martelli, A. Masserot, M. Mazzone, F. Menzinger, L. Milano, C. Moins, J. Moreau, N. Morgado, B. Mours, F. Nocera, C. Palomba, F. Paoletti, S. Pardi, A. Pasqualetti, R. Passaquieti, D. Passuello, F. Piergiovanni, L. Pinard, P. Poggiani, M. Punturo, P. Puppo, S. van der Putten, K. Qipiani, P. Rapagnani, V. Reita, A. Remillieux, F. Ricci, I. Ricciardi, P. Ruggi, G. Russo, S. Solimeno, A. Spallicci, M. Tarallo, M. Tonelli, A. Toncelli, E. Tournefier, F. Travasso, C. Tremola, G. Vajente, D. Verkindt, F. Vetrano, A. Viceré, J.-Y. Vinet, H. Vocca, and M. Yvert

Abstract—The VIRGO experiment for the detection of gravitational waves is a big challenge both for physics and for technology. In particular, to satisfy the stringent requirements on the alignment and position of its suspended optical components to keep the detector at its point, a very complex distributed and supervised control system has been implemented. The current constraints are about 10^{-10} m RMS for the longitudinal control (“Locking”) and 10^{-9} rad RMS for the angular degrees of freedom (“Alignment”). These requirements are satisfied by means of a specially designed hierarchical architecture for the local control system. It is necessary for managing the hard task of filtering all the environmental noises that limit the sensitivity of the interferometer. On the other end, the interferometer is supervised by a distributed global control system to maintain the detector fully operational. In this paper we describe the status of the real-time distributed control system of the Virgo interferometric detector of Gravitational waves, its performances and planned improvements.

I. INTRODUCTION

VIRGO [1] is a French–Italian experiment aimed at the direct detection of gravitational waves (see e.g., [2]). It is based on a km scale Michelson interferometer with Fabry–Perot cavities in the arms and light recycling technique in order to improve its sensitivity. Together with the two American LIGO interferometers [3] and the German–British GEO [4] it forms a network of interferometric detectors for gravitational wave searches.

It can be shown that a perfect Michelson interferometer (defined by its arm length L and illuminated by a laser with a power P and a wavelength λ) reaches its maximum sensitivity when it is tuned on the dark fringe. In the optimal case, the sensitivity to

gravitational waves is limited by the photon counting statistics (shot noise):

$$h_{\text{shot}} = 1/2\pi L \sqrt{hc\lambda/P\Delta t}$$
, being h_{shot} the minimum detectable length perturbation $2\Delta L/L$ due to shot noise, h the Planck constant, c the speed of light, P the laser power, L the arm length and Δt the observation time. Thus, the longer is the arm length, the better is the sensitivity. In ground based interferometers, the arm length cannot go above the kilometer scale because of the land configuration and the cost of the needed infrastructure. The Virgo interferometer arms are 3 km long (see Fig. 1). In order to increase the optical path within a given physical dimension, two Fabry–Perot cavities are inserted in the arms. When the Fabry–Perot cavity is resonant, the optical length is related to the physical path by: $l_{\text{opt}} = l_{\text{phys}}(2F/\pi)$, where the Finesse, F , is a function of the cavity mirrors’ reflectivities and gives a measure of the “sharpness” of the cavity resonance [5]. The Finesse of VIRGO Fabry–Perot cavity is $F_{fp} = 50$.

Since in dark fringe condition most of the light is reflected back to the laser, an additional mirror—the recycling mirror—is added between the beam splitter and the laser, giving rise to another cavity: the recycling cavity that “recycles” into the interferometer the back reflected power. The Finesse of this new cavity, F_{Rec} , is related to the total losses of the interferometer and, in the case of VIRGO, is around 50 (as a comparison, in LIGO [6] is $F_{fp} = 205$ and $F_{\text{Rec}} = 50$).

II. CONSTRAINTS

The foreseen sensitivity imposes the Fabry–Perot arms and the recycled cavity to be resonant, and the interferometer locked on dark fringe. The longitudinal mirror control to achieve these conditions is called *Locking*.

The conditions to keep the cavities locked are that the fluctuations on the cavities’ lengths must be less than 1/10 of the full width at half maximum of the resonance. This leads to

Manuscript received May 11, 2007, revised October 29, 2007.

Please see the Conclusion section of this paper for the author affiliations.

Color versions of one or more of the figures in this paper are available online at <http://ieeexplore.ieee.org>.

Digital Object Identifier 10.1109/TNS.2007.912887

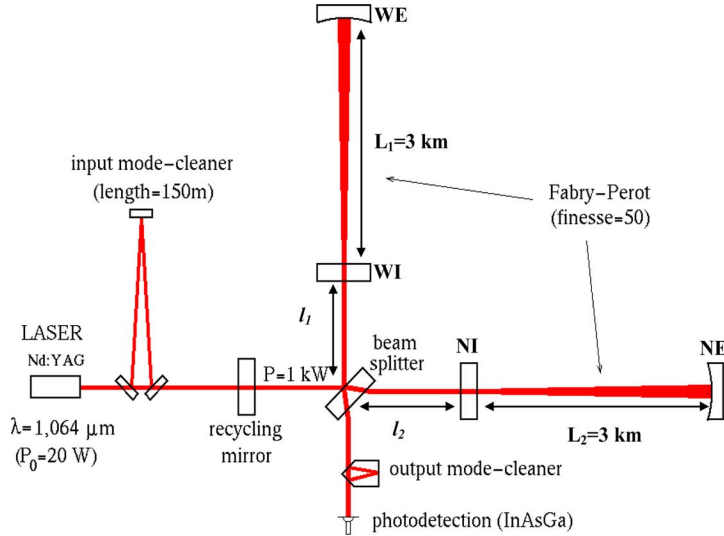


Fig. 1. Virgo interferometer optical configuration. The light path inside the arms is increased with the Fabry-Perot cavities formed by the input mirrors and the end mirrors, The back-reflected power is re-injected by the recycling mirror.

the constraints on the Fabry-Perot longitudinal control: $\delta L_i \leq \lambda/4F_{fp} = 5 \cdot 10^{-9}$ mm, and on the Recycling cavity control: $\delta l_i \leq \lambda/4F_{rec} = 5 \cdot 10^{-9}$ m [7]. Even stricter is the condition on the dark fringe due to the power fluctuations of the laser. These fluctuations couple to the dark fringe offset and can overrun the shot noise limit. If one wants the length fluctuations to be lower than the shot noise fluctuation, considering an impinging power on the beam splitter of 1 kW and a power fluctuation $\Delta \dot{P}/P = 10^{-8}/\sqrt{\text{Hz}}$, this constrains the mirrors' positions (see Fig. 1) to be such that $l_d = l_2 - l_1 + 2(F_{fp}/\pi)(L_2 - L_1)$ must be within 10^{-10} m [7].

For the Fabry-Perot cavity to work properly, the cavity mirrors must be aligned. The laser direction jitter couples to the static misalignment of the mirrors and the induced noise can limit the interferometer sensitivity. An analytic calculation leads to the constraints on the Fabry-Perot and recycling mirror angular control: $\delta \theta_{FP_end} < 3 \cdot 10^{-9}$ rad; $\delta \theta_{FP_input} < 2 \cdot 10^{-8}$ rad; $\delta \theta_{rec} < 10^{-7}$ rad [7].

It is clear that to maintain these conditions on all the mirrors on a kilometer distance is a very complex task, that implies also the mirrors must be as much isolated as possible from all the environmental noises (seismic, tidal, electromagnetic, etc). The goal is achieved by the combination of a mechanical isolation from the ground motions, local mirror controls and a global interferometer control system.

An Environmental Monitoring (EM) system [8], monitors all the environmental quantities that can have an effect on the interferometer output with the help of seismic, lightning, wind, temperature, acoustic, humidity and EM sensors widespread all over the experimental areas. Information from EM (typically seismic and wind) is used to tune some parameters in the local controls.

III. SUSPENSIONS AND LOCAL CONTROLS

A. Superattenuator and Hierarchical Control

To isolate the mirrors from ground motions within the detection band (~ 4 to 10^4 Hz, being the lower limit given by

thermal noise and by the height of the suspension), they are suspended to a multi pendular structure: the *superattenuator* (SA) [9], as shown in Fig. 2. The first stage is formed by an *inverted pendulum* (IP) to the top of which, five mechanical filters are suspended equipped with an anti-spring [10] to dump vertical oscillations. The IP is composed of three flex joints, each supporting a leg. At the top, the three legs are connected to a rigid table by means of small flexures. The IP has two translational modes and one torsional mode. Each pendular stage, acts as a 2nd order low-pass filter. To the last stage (the so called filter 7), an anvil shaped steel stage, the so called “marionette,” is suspended by a steel wire. The payload, suspended from the marionette, is formed by the mirror and by an aluminum reference mass, independently suspended behind the mirror [11].

The full chain is characterized by very low frequency normal modes (all are in the range 0.04–3 Hz).

In order to get the lock conditions, besides providing a passive filtering of the seismic mechanical vibrations, the SA is designed to allow an active control of the mirror position over a very large dynamic range [12]. To extend the detection band down to 4 Hz, stricter limits on the actuators noise are demanded. In particular, the actuation stages close to the mirror must be free from seismic noise, i.e they must be suspended. Control forces are exerted at three actuation points (see Fig. 2).

- The Inverted pendulum top stage is provided by accelerometers and position sensors [13], [14]. Magnetic actuators centre the chain and use the sensor signals for low frequency three dimensional active damping of the resonances of the SA;
- the Marionette, by means of magnetic actuators, allows moving the payload with respect to the last stage [11];
- the reference mass, equipped with coils that act on the mirrors.

The force on the three actuation points is exerted in different frequency bands as explained in [15]: below 10^{-2} Hz on the top stage, between 10^{-2} and 5 Hz on the marionette, and from 5 to 50 Hz on the reference mass. Moreover, since reaching the work

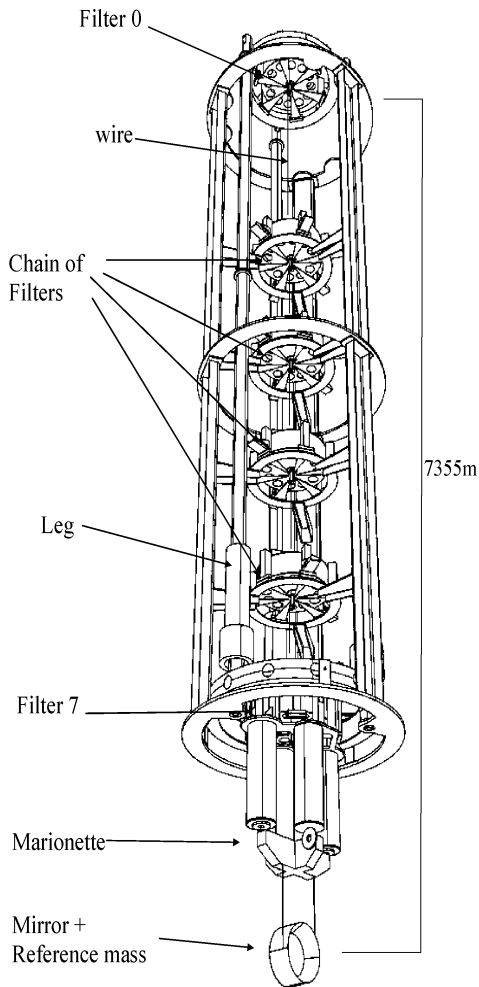


Fig. 2. Multipendular suspension of Virgo. The three legs are free to oscillate as an inverted pendulum. The top stage is equipped with accelerometers and position sensors, coil magnet actuators and an anti-spring to dump vertical oscillations. Five pendular stages are suspended, each equipped with an anti-spring. The payload is suspended to the last stage by the so called marionette.

point needs a larger force than maintaining it, a high gain chain is used in the lock acquisition phase while a low gain chain is used in lock conditions.

In the IP control, three linear variable differential transducers (LVDT) [13] and three accelerometers [14] placed on the top-stage of the IP measure respectively the position of the IP relatively to the external frame and the acceleration in the x , y (transverse translations of the chain suspension point in the horizontal plane) and θ (rotation of the IP top-stage around the vertical direction) degrees of freedom. The obtained error signal matrix is diagonalized in order to reduce the system from a Multiple Input Multiple Output (MIMO) to three Single Input Single Output (SISO). Then, for each d.o.f., the diagonalized accelerometer and LVDT signals are blended using a low pass filter and high pass filter in order to minimize the re-injection of seismic noise and build up the signal sent to three coil-magnet actuators which correct the x , y and θ fluctuations.

The diagonalization and filtering operation are made on a custom digital signal processing unit (DSP) [16] based on Motorola DSP96002 capable to implement Infinite Impulse Response (IIR) filters with 8 poles and 8 zeros in about 1 mi-

crosecond. In addition to IIR filters implementation, the DSP implements signal generators, matrix multiplication, switches, comparators with hysteresis and many others. The sustained computational power available is about 40 Mega Floating Point Operations per Second (MFLOPS).

The need of a custom DSP was dictated by the absence of commercial boards with the desired performance and the needed I/O at the time the VIRGO control system was designed.

The Virgo control system runs at 10 kHz in order not to have excessive phase rotation at frequencies of interest (we control the suspended masses up to 100 Hz). With a sampling frequency of 10 kHz, the input to output delay of our DSP system (taking into account the delay introduced by the antialiasing filter in front of the ADC and the corresponding low pass filter behind the DAC) is about $540 \mu\text{s}$. This delay will introduce phase rotation of about 20° at 100 Hz, low enough for our purposes. The timing is given by the global VIRGO timing system [17].

B. Local Control

Proper detector operation needs a pre-alignment and a mirror angular control. This task is accomplished by the *local control* [11] consisting of a CCD camera [17] and a laser diode injecting light onto the mirror inside each tower vacuum tank. Both the camera and the laser are on the ground, outside the tower: the laser is injected through an optical fiber and the camera monitors the light spot through a window. Six error signals, x , y , z , θ_x , θ_y , θ_z are referred to the mechanical ground of the CCD-camera and reconstructed. A dedicated read-out board was developed in order to use this CCD-camera for real-time applications in the standard VME crates of Virgo. The CCD-chip is a scientific grade square 512×512 pixel matrix with $7.7 \times 7.7 \text{ mm}^2$ surface. The pixel width is $15 \mu\text{m}$. The pixel, clock is set at 20 MHz and the system provides a digital signal through an 8-bit ADC. The image is gathered and converted in 16 ms. Thus, the maximum speed is 60 frames/s. The frame grabbing, triggered by an external timing control, is a key feature of this system integrated in the real-time local control standard crate of Virgo. The accuracy of the CCD position sensing is roughly 10 nm RMS, on the surface of the CCD chip, with a spot diameter of 30–300 μm . The readout system described above was designed to accomplish two main tasks:

- (A) the control of large angular offsets or oscillations in the pre-alignment phase (coarse-mode);
- (B) control during the locking and operation phases (fine-mode).

The pre-alignment step is accomplished by monitoring four ceramic markers glued on the mirror holder illuminated with a halogen lamp. Differential signals are derived from these measurements at 50 Hz and passed to a DSP until the control accuracy provides 100 μrad RMS and 100 μm rms. Then, the fine error-signal computation of θ_x and θ_y , obtained by a linear combination of the variations along the two coordinates read by two Position Sensing Devices (PSD) looking at the reflected laser beam, automatically replaces the coarse computation and the halogen illuminator is switched off. If during the operation the control is switched back from the fine to the coarse-mode, the calibration and the offset of coarse signals are automatically updated by matching the last (more accurate) values provided by the fine measurement. In Fig. 3 the main elements of

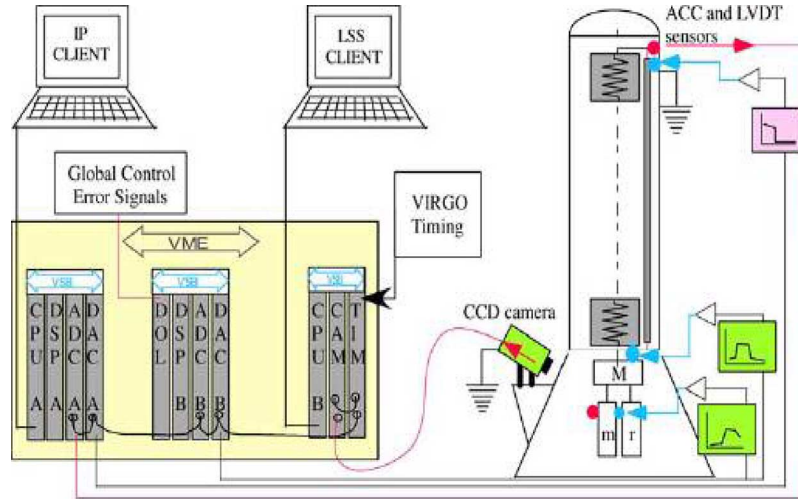


Fig. 3. Schematic view of local control chain. Read-out and actuation points are shown. The actuation forces are exerted at three different stages in different frequency bands: a tidal control (0 – 0.01 Hz) on filter 0, a marionette control (0.01 – 5 Hz), and a mirror control (5 – 50 Hz) on the reference mass.

the local control chain are shown. The VME crate is divided in two sections, each equipped with a dedicated CPU board (coded as A and B). The main process running on the CPU-A is the DSP-server, a software program designed to allow communication between the higher level supervising software and the software on the digital signal processing boards (DSP-A and B) that control a set of ADC (16 bit ± 10 V with a noise floor of $4 \mu\text{V}/\sqrt{\text{Hz}}$) and DAC (20 bit ± 10 V; $200 \text{ nV}/\sqrt{\text{Hz}}$) boards. Both DSP units are also programmed to send data to the data acquisition system (DAQ) running elsewhere and to receive signals from the Global control system through digital optical link boards (DOL) [18].

IV. GLOBAL CONTROL

The global control [7] is the system in charge of collecting data from the photodiodes implied in locking and alignment, compute the correction signals and send them to the proper actuators to keep the interferometer at its working point. The Locking loop runs at 10 kHz while the Alignment one is synchronized at 500 Hz. A higher bandwidth is needed for Locking mainly for the lock acquisition step where feedbacks with high unity-gain frequency are needed. All data are also sent to the DAQ at the data acquisition frequency of 20 kHz to be stored in the Raw Data frames, being this latter frequency determined by the Virgo detection band that extends up to 10 kHz.

A. Locking

The goal of a lock acquisition procedure is to bring the ITF to its working point, by controlling its independent longitudinal lengths.

Four lengths must be controlled [20] (with reference to Fig. 4).

1. MICH = $l_2 - l_1$.
2. PRCL = $l_{\text{rec}} + (l_2 + l_1)/2$.
3. CARM = $L_2 + L_1$.
4. DARM = $L_2 - L_1$.

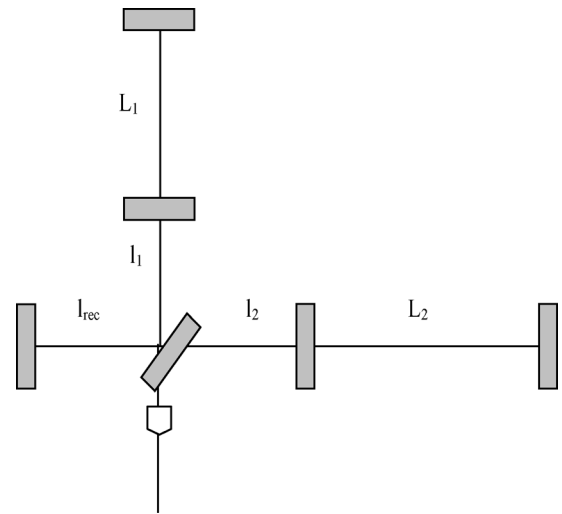


Fig. 4. Virgo locking procedure: the four lengths to be controlled to lock the interferometer are linear combinations of the arm lengths L_i and the power recycling and Fabry–Perot cavity lengths.

For the ITF locking a novel strategy, called *Variable Finesse Locking* [20] has been adopted. The basic idea is that the ITF is locked on the half (grey) fringe and then brought sequentially to the dark fringe through several steps. During those steps the control scheme is changed.

The lock acquisition procedure embeds this strategy and consists of two main sequences:

1. pre-alignment sequence;
2. locking sequence.

All this is implemented by an Automatic Locking Procedure (ALP) [21]. The basic concept underlying ALP is to use the data acquired by the DAQ and to compute, on a standard workstation, the state of each subsystem by processing the collected channels related to it. According to the subsystem state, actions can be performed using the system calls or directly sending messages over the network.

The ALP server uses the DAQ framework to access the data and to report on the performed actions. It uses the *macro* concept to define a set of code related to the same automation phase and a script language to define the macros' content.

A set of macros align the direct beams inside the arms, lock independently the North and West cavities and execute a coarse Power Recycling mirror alignment with respect to the arm cavities mirrors.

Once acquired, the locking is maintained by the Global Control Locking loop.

One of the major Locking loop constraints is to be perfectly synchronized at 10 kHz. Any delay larger than some microsecond makes the system unstable, so, every 100 μ s, the Global Control performs the same series of tasks. First of all, the Global Control checks the time stamp (given by the Virgo Timing system [17]) of the data in order to insure the synchronization and controls that the photodiode value is inside a defined range in order to avoid overflow problems. Then the lengths are estimated via an optical matrix and translated into individual mirror displacements. This splitting between suspensions can be done using a static driving matrix. However, the driving part can include a splitting in different frequency bands in order to use the natural mechanical gain of the suspensions at some frequencies or to avoid frequency regions where a given suspension has a notch in its transfer function. Once computed, all corrections and triggers are sent using optical links to the suspensions and the Input Bench crates.

1) *Error Signals for the Locking*: The Pound–Drever method [22] has been used to control the length of a Fabry–Perot cavity illuminated by a laser. The technique consists of phase modulating the incoming beam at a frequency chosen in order to have the sidebands anti-resonant when the carrier is resonant. Then, the error signals are obtained by looking at the demodulated components of the reflected and transmitted beams. A length modification induces a beating between the carrier and the side-bands which is the source of the error signal. Near the resonance, the error signal depends linearly on the displacement toward the resonance and the slope is fully determined by the optical characteristics of the cavity.

B. Alignment

The current design requirements for the Automatic Alignment (AA) system [23] have been derived from noise computations for the couplings of the angular motion of the mirrors with high frequency beam jitter or with a constant miscentering. In brief, if we assume, for example, that the beam is centered on the end mirror with an accuracy of 1 mm, then the requirement for the residual RMS motion of the end mirror is 10^{-6} rad. However, more stringent requirements are obtained from computing the coupling with the input beam jitter. Taking into account a jitter of the input beam of the order of 10^{-11} rad/ $\sqrt{\text{Hz}}$, the limits for the residual RMS motion of all mirrors are:

- 10^{-7} rad RMS for the recycling mirror;
- 2×10^{-8} rad RMS for the input mirrors;
- 3×10^{-9} rad RMS for the end mirrors.

The Alignment feedback loop runs at 500 Hz. The Global Control accesses the signals coming from the photodiodes (9 quadrants, each giving 2 RF signals and 1 DC, i.e 27 signals per an-

gular direction), and uses the reconstruction matrices to get the mirror angular position. The reconstruction matrices are computed by a χ^2 minimization technique [23] from the optical matrices, i.e., matrices whose elements are the low-frequency limit of the transfer function between a mirror motion and a quadrant diode demodulated signal. The optical matrices are measured periodically by injecting sinusoidal excitation at the level of marionette. Then, the AA error signals are serviced by the Global Control and sent to the suspensions and the input bench.

Since there is only one channel from Global control for each suspension for both the longitudinal and angular control, the alignment corrections are sent to suspensions at the locking frequency (10 kHz) although they are refreshed at the alignment frequency (500 Hz).

1) *Angular Error Signals*: When a perfect Gaussian beam (pure TEM₀₀) impinges on a tilted mirror, some high order modes are generated. If the tilt angle is much less than the beam divergence, in practice, only the first mode (TEM₁₀ or TEM₀₁) is generated. The error signal used for the control is proportional to the product TEM₀₀ \times TEM₁₀ which gives no signal on a standard photodiode. So, it is necessary to use a quadrant photodiode to extract the spatial information, using the differences between horizontal and vertical quadrants.

For the Virgo Alignment a differential wave front sensing technique (the Anderson-Giordano technique [24]) is adopted. For each beam, two quadrant photodiodes (QPD) sense the wave front change at the laser waist position and at the far end. The modulation frequencies for Alignment and Locking are identical. Once the interferometer is longitudinally locked, the angular error signals are related to the various misalignments through a matrix like in the longitudinal case.

In Fig. 5, the Global control read-out schematic is shown, while in Fig. 6, the main actors in Global Control chain and their interconnection are outlined: Signals are sent to the input bench control for the second stage of laser frequency stabilization (SSFS) [26].

C. Global Control Hardware Architecture

The Global Control hardware consists of three components: a crate housing the hardware dedicated to the Locking feedback loops, a second crate for the Alignment control loop and a workstation monitoring the system.

The philosophy underlying the hardware choices is to split the functions into mostly independent CPUs and processes in order to minimize the interference on the fastest feedback loop and to build a flexible architecture which can easily evolve.

The technical constraints for the global control are given by the large number of signals it has to read from a large number of boards (25 words on 8 boards for locking and 83 signals on 3 boards for alignment), the correction signals to be written (39 for locking and 17 for alignment), the data to be transferred between systems, and the control loop timing.

The signals are acquired by 18 bit, ± 10 V ADCs with a noise floor of $1 \mu\text{V}/\sqrt{\text{Hz}}$, and delivered by 20 bit DAC with a noise floor of $200 \text{ nV}/\sqrt{\text{Hz}}$.

The standard bus of choice for VIRGO is VME [25] with VSB (VMEBus Subsystem Bus [27]) for high speed data transfer. VSB is hosted on the same crates of VME via piggy-back cir-

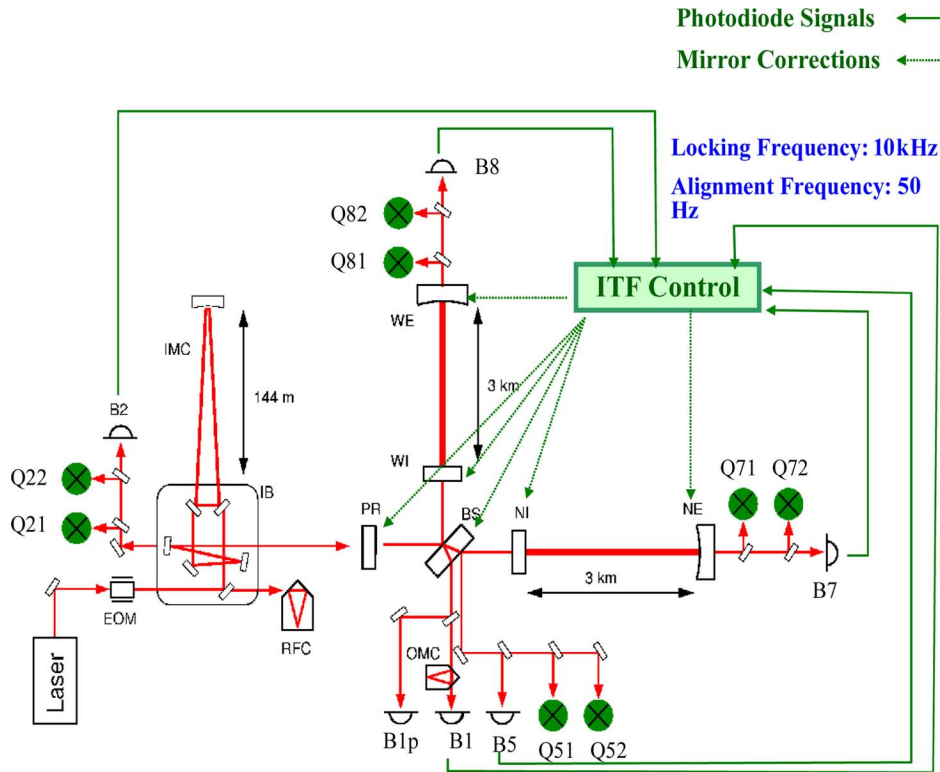


Fig. 5. Schematic view of the global control locking and alignment. The photodiodes used for longitudinal (labelled with B, beam) and angular (labelled with Q, quadrant) controls are shown. The input signal is modulated and the photodiode signal is demodulated, giving 2 RF and one DC signal for each photodiode or quadrant sector.

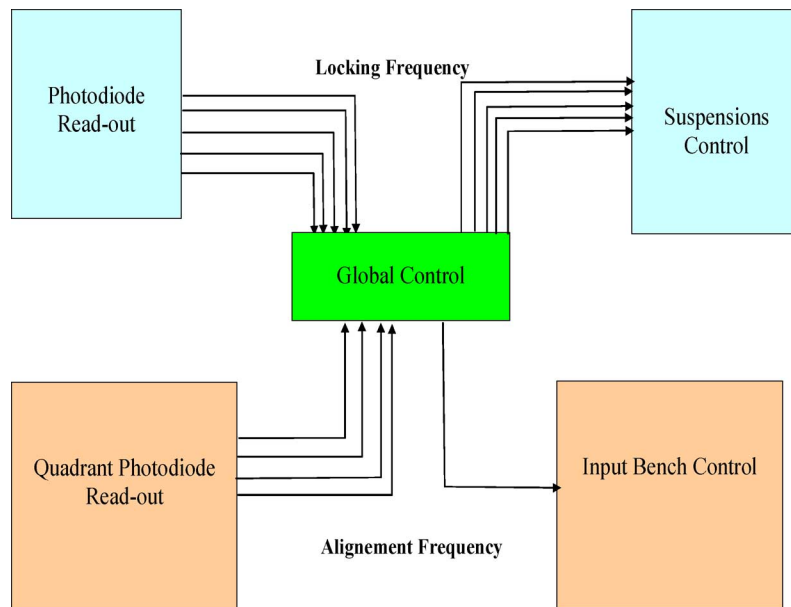


Fig. 6. Actors of the virgo control. The control chain is composed by the photodiode readouts, the global control, the suspensions controls and the input bench control. Photodiode read-out and suspension controls work at the locking frequency (10 kHz), quadrant read-out and alignment control at the alignment frequency (500 Hz).

cuits. The VME CPU used by global control is the RIO8062 [28] by CES [29], based on Motorola PowerPC604 CPU and a custom designed VME to PCI bridge. The operating system is LynxOS by LinuxWorks [30], a real-time Unix-like POSIX conformant operating system for embedded applications, in version 2.5.1.

The various subsystems of VIRGO exchange data via optical fibers, connected through a custom Digital Optical Link (DOL) board [31]. It is a VME/VSB module capable of sending small amount of data (some kByte) in a point-to-point connection over distances up to 3.2 km with nominally ~ 300 ns latency. All the VIRGO subsystems are synchronized by means of a cen-

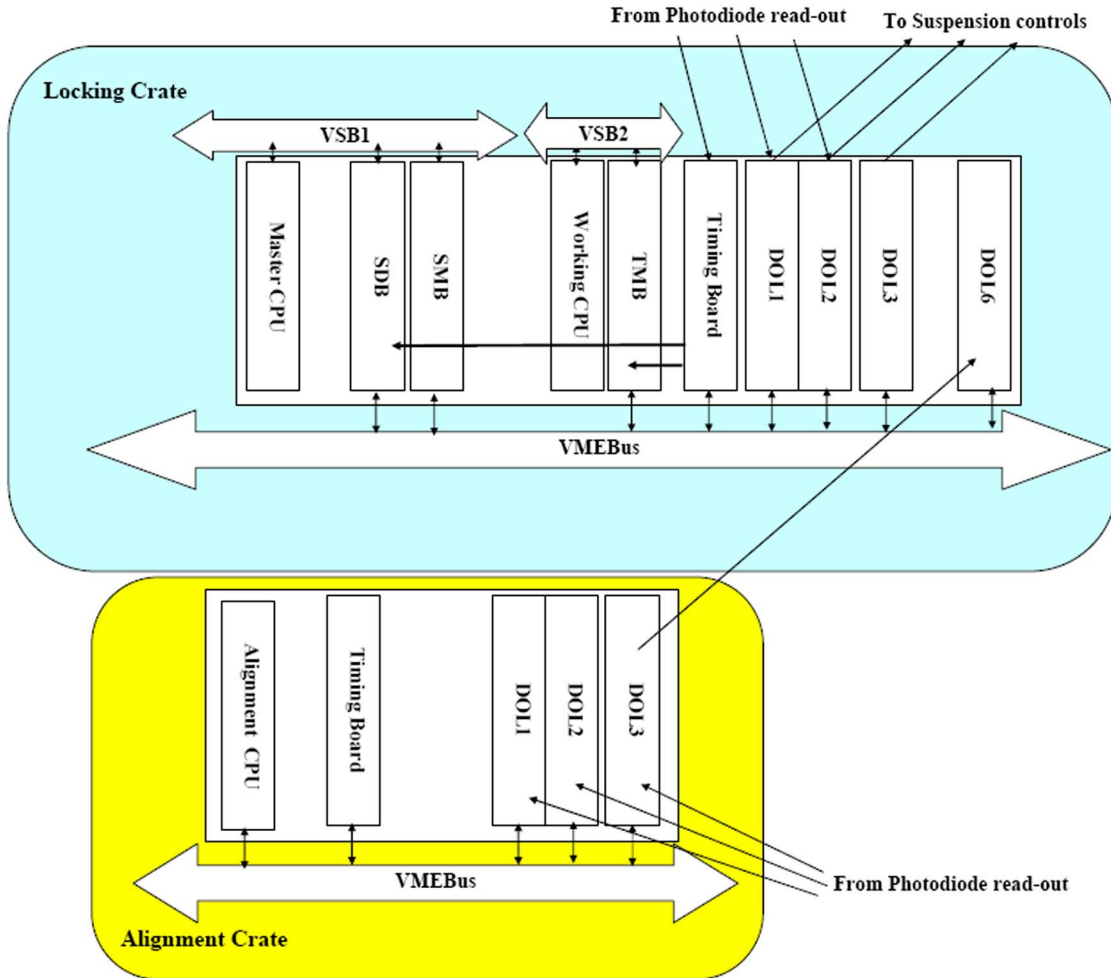


Fig. 7. Schematic view of RIOT global control crates with their connections. The two crates are connected through an optical fibre from DOL3 on alignment crate to DOL6 on the locking crate.

tral clock derived from a GPS receiver ([32] $1 \mu\text{s}$ time accuracy) and custom timing boards. The central clock is delivered through optical fibers to the different buildings and the timing boards convert it into TTL signals and VME bus interrupts for local use. The maximum time shift between the clocks in two buildings is estimated to be 10 ns. The GPS timing ensures that the experiments in the network (VIRGO, LIGO and GEO) are synchronized within 1 ms so that the angular direction of a gravitational wave can be estimated from the time delay in different locations.

To reach the desired performance it has been necessary to design a Transparent Memory Board (TMB) [33] that allows the CPUs to read/write at a single address and acts as a transparent bridge between the VSB and the VME for the distribution of data, triggered by the timing signal. Moreover a custom VSB LynxOS driver has been written, because the CES driver was poorly performing for the needs of Global Control.

With the described hardware, the Global Control can match the 10 kHz constraint, but the CPU time remaining for other operations such as monitoring is not enough. Thus a SPY Data Board (SDB) [7], [34] has been built, to sniff the data read/written by the TMBs on the VME and present them on the VSB

in such a way that another CPU, dedicated to locking monitoring, can access data without disturbing the locking loop.

In Fig. 7, a schematic view of the Real Time Global control (RIOT) is shown. The SMB [7], [34] is a shared memory (dual port VME/VSB) that allows the “working” CPU to access commands and writes status from/to the master.

D. Global Control Software Architecture

All the VIRGO on-line applications are built following the client-server scheme.

The Global Control is composed by various servers, as shown in Fig. 8. Two main processes are in charge of handling the Alignment and the Locking fast loops, a supervisor process and monitoring processes.

The GC Supervisor [34] handles the whole Global Control in a centralized way and its graphical user interface gives information about the servers’ state and allows steering the final state machines associated to each server. All other processes are dedicated to monitoring, and share the data with one another on the same CPU through a shared memory, in order to minimize the interference between the monitoring and control processes.

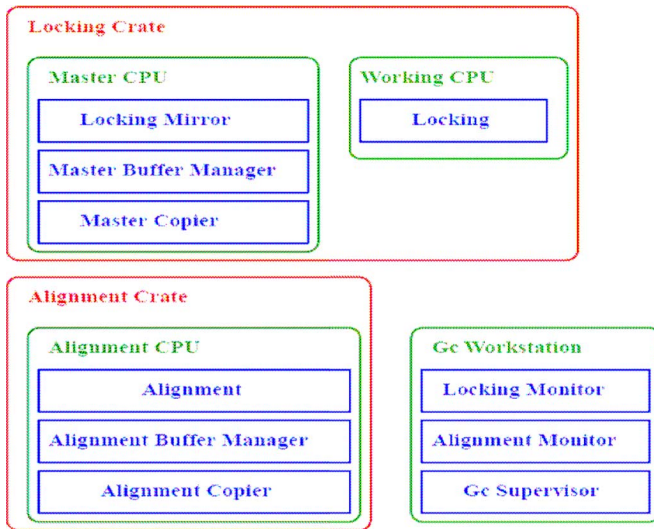


Fig. 8. Schematic view of global control software architecture with the processes running on the CPUs and the GC workstation. The locking and alignment processes are complex multi-threaded applications with threads accessing memory in concurrency to one another and with the copier A buffer manager is needed to handle the shared memory access.

To manage accesses to the shared memory with a producer-consumer model, a buffer manager has been developed, capable of handling several producers and consumers at the same time.

Once the Copier consumer has acquired the data from the buffer manager, it sends them to the monitoring processes via TCP/IP, with the help of the Cm package [35]. This package has been built with the aim to permit the communication between the processes hiding to the user the complexity of the TCP/IP programming.

The Locking server has to handle the data exchange between locking crates with the DOLs and apply the control algorithms. The locking algorithm is logically split in four parts.

1. Sensing: Computes the lengths from the photodiodes signals. Although this is rather simple near the working point, during the lock acquisition procedure it is not simply based on an optical matrix but requires an algorithm that needs the optical matrices to be estimated at each step of the procedure and inverted at the Locking frequency.
2. Filtering: Applies the time domain correction filters to the lengths computed by sensing.
3. Boost: Applies several integrator filters to suppress the DC component of the error signal. It is used only after the lock acquisition phase is completed.
4. Driving: The various filtered lengths are distributed to the mirrors according to the driving matrix, supplied by the user.

All the free parameters of the algorithm (optical gain, filter parameters, etc.) are stored in the VIRGO on-line database [36], as well as the history of parameter changes, so that any change in the behavior of the algorithms can be applied and reverted without modifying the code.

The alignment server is built with the same criteria, but consists of only two parts: sensing and filtering.

V. FUTURE DEVELOPMENTS

The suspension control, in use since 1998, is now approaching its limits in terms of both computational power and converter dynamical range. A new control system [15], now under development, foresees multi-DSP computing units, faster and higher resolution ADCs and DACs, and highly dynamic power drives for coil magnet pairs. Operations up to 100 kSamples per second in high resolution or 2 MSamples per second at lower resolution will be available with the new system.

The new DSP board shall be constituted by a carrier VME board hosting up to three PMC (PCI Mezzanine Card) [37] mezzanine boards on its front side, while the back side can host link to PCI-Express [38] CPU modules or external CPU boards. It is based on the Analog Devices SHARC ADSP-21160N [39] at 100 MHz clock speed, Each mezzanine contains six DSP devoted to different tasks, and their mutual connection topology reflects it.

In parallel to the new DSP architecture, a new coil driver scheme has already been tested on the suspension [40] and is currently in use. This scheme is based on the use of two different chains for lock acquisition and linear lock phases, using two different DACs: DAC1 and DAC2. In lock acquisition a higher current is needed and some more noise is tolerated; this is obtained with DAC1 and a transconductance amplifier. After the lock is acquired, DAC1 is switched off and DAC2 is enabled to keep the lock. A further noise reduction is achieved in this second chain by inserting a digital high-pass filter (emphasis) before converting the signal into analog domain for then low-pass filtering in the coil driver. De-emphasis filter can be inserted in front of coil driver.

To improve the immunity to electromagnetic noise, the ADC and DAC boards, presently in the VIRGO data acquisition room and connected to the coil drivers with 30 m of cable, will be hosted on-board the new coil driver, near the actuation point. The new coil driver will host also a digital optical link to transmit digital data to data acquisition room.

VI. CONCLUSION

The high demanding constraints of the VIRGO experiment, gave rise to the necessity of a very complex supervised and distributed control system.

The VIRGO Control system is constituted by local controls at each suspension, supervised by a global control system that uses the interferometer output to keep the interferometer locked and aligned. The procedures to attain the locking state, are completely automated by the Automatic Locking Procedure. The whole system is synchronized by a GPS based timing system.

To implement the VIRGO control system, several digital VME/VSX boards and a DSP have been designed and produced at the time the control has started to work. With the available technology VIRGO is able to approach the desired sensitivity, and plans to reach it in the next year.

At present, the technology allows improvements that are already in an advanced stage of development.

P. Amico, L. Bosi, F. Cottone, A. Dari, L. Gammaitoni, F. Marchesoni, M. Punturo, F. Travasso, and H. Vocca are with the INFN-Sezione di Perugia, Università di Perugia, 06123 Perugia, Italy.

M. Alshourbagy, L. Barsotti, S. Bigotta, S. Birindelli, C. Bradaschia, S. Braccini, G. Cella, C. Corda, M. del Prete, A. Di Virgilio, I. Ferrante, F. Fidecaro, F. Frasconi, A. Gennai, A. Giazotto, M. Mantovani, R. Passaquieti, D. Passuello, R. Poggiani, M. Tarallo, M. Tonelli, A. Toncelli, C. Tremola, and G. Vajente are with the INFN-Sezione di Pisa, Università di Pisa, 56121 Pisa, Italy.

F. Antonucci, P. Astone, A. Corsi, S. Frasca, E. Majorana, C. Palomba, P. Puppo, P. Rapagnani, and F. Ricci are with the INFN-Sezione di Roma, Università La Sapienza, 00185 Rome, Italy.

S. Aoudia, F. Bondu, A. Brillé, E. Chassande-Mottin, F. Cleva, J.-P. Coulon, B. Dujardin, J.-D. Fournier, H. Heitmann, M. Laval, C. N. Man, A. Spallicci, and J.-Y. Vinet are with the Département Artemis, Observatoire de la Côte d'Azur, 06304 Nice, France.

S. Avino, E. Calloni, R. De Rosa, L. Di Fiore, A. Eleuteri, F. Garufi, L. Giordano, L. Milano, S. Pardi, K. Qipiani, I. Ricciardi, G. Russo, and S. Solimeno are with the Università degli Studi di Napoli Federico II, Napoli, Italy, and also with the INFN Sezione di Napoli, Napoli, Italy (e-mail: fabio.garufi@na.infn.it).

D. Babusci and G. Giordano are with the Laboratori Nazionali di Frascati, INFN, 00044 Frascati, Italy.

G. Ballardin, R. Barillé, F. Carbognani, R. Cavalieri, N. Christensen, E. Cuomo, V. Dattilo, M. Evans, I. Fiori, A. Freise, E. Genin, S. Hamdani, S. Hebri, D. Huet, P. La Penna, B. Lopez, J. Marque, F. Menzinger, C. Moins, F. Nocera, A. Pasqualetti, and P. Ruggi are with the European Gravitational Observatory, 56021 Cascina, Italy.

M. Barsuglia, M. A. Bizouard, V. Brisson, F. Cavalier, A.-C. Clapson, M. Davier, P. Hello, S. Kreckelbergh, and N. Leroy are with the Laboratoire de l'Accélérateur Linéaire, IN2P3/CNRS-University de Paris-Sud, 91898 Orsay, France.

F. Beauville, D. Buskulic, R. Gouaty, D. Grosjean, S. Karkar, N. Letendre, F. Marion, A. Masserot, B. Mours, E. Tournefier, D. Verkindt, and M. Yvert are with the Laboratoire d'Annecy-le-Vieux de Physique des Particules, 74941 Annecy-le-Vieux, France.

C. Boccarda, V. Lorient, J. Moreau, and V. Reita are with ESPCI, 75231 Paris, France.

T. S. Bauer is with the INFN-Sezione di Pisa, Università di Pisa, 56121 Pisa, Italy, and also with the National Institute for Nuclear Physics and High Energy Physics, NL-1009 DB Amsterdam, The Netherlands, and the Vrije Universiteit, NL-1081 HV Amsterdam, The Netherlands.

E. Campagna, E. Cesarini, G. Guidi, M. Lorenzini, G. Losurdo, F. Martelli, M. Mazzoni, F. Piergiovanni, F. Vetranò, and A. Viceré are with the INFN-Sezione di Firenze/Urbino, 50019 Sesto Fiorentino, Italy, and also with the Università di Firenze, 50125 Firenze, Italy, and the Università di Urbino, 61029 Urbino, Italy.

R. Flaminio is with the Laboratoire d'Annecy-le-Vieux de Physique des Particules, 74941 Annecy-le-Vieux, France, and also with the European Gravitational Observatory, 56021 Cascina, Italy.

J.-M. Mackowski, N. Morgado, L. Pinard, and A. Remillieux are with the LMA, 69622 Villeurbanne, France.

F. Paoletti is with European Gravitational Observatory, 56021 Cascina, Italy, and also with INFN-Sezione di Pisa, Università di Pisa, 56121 Pisa, Italy.

J. F. J. van der Brand and S. van der Putten are with the National Institute for Nuclear Physics and High Energy Physics, NL-1009 DB Amsterdam, The Netherlands, and the Vrije Universiteit, NL-1081 HV Amsterdam, The Netherlands.

REFERENCES

- [1] Final Design Rep., The Virgo Collaboration., 1997, Virgo note VIR-TRE-DIR-1000-13.
- [2] K. S. Thorne, E. W. Kolb and R. Peccei, Eds., "Gravitational waves," in *Proc. Snowmass Summer Study on Particle and Nuclear Astrophysics and Cosmology*, Singapore, 1995, pp. 160–84.
- [3] LIGO Laser Interferometer Gravitational-Waves Observatory. [Online]. Available: <http://www.ligo.caltech.edu>
- [4] GEO600 The German-British Gravitational Wave Detector. [Online]. Available: <http://geo600.aei.mpg.de/>
- [5] M. Born and E. Wolf, *Principle of Optics: Electromagnetic Theory of Propagation, Interference and Diffraction of Light*, 7th ed. Cambridge, U.K.: Cambridge Univ. Press, 1999.
- [6] M. Rakhmanov and A. Arodzero, Dynamics of Fabry–Perot Resonators With Suspended Mirrors I. Nonlinear Coupled Oscillators, 1998, LIGO-T970229-R, arXiv:physics/9809038v1.
- [7] N. Arnaud *et al.*, "The global control of the VIRGO experiment," *Nucl. Instrum. Meth. A*, vol. 550, pp. 467–489, 2005.
- [8] A. Anastasio, F. Barone, A. Eleuteri, F. Garufi, and L. Milano, "The environment monitoring of the VIRGO antenna for gravitational wave detection," in *Proc. 3rd Edoardo Amaldi Conf.*, Pasadena, CA, Jul. 12–16, 1999, vol. 523, p. 461.
- [9] F. Acernese *et al.*, "Measurement of the seismic attenuation performance of VIRGO superattenuator," *Astroparticle Phys.*, vol. 23, pp. 557–565, 2005.
- [10] A. Bertolini, G. Cella, R. DeSalvo, and V. Sannibale, "Seismic noise filters, vertical resonance frequency reduction with geometric anti-springs: A feasibility study," *Nucl. Instrum. Meth. A*, vol. 435, pp. 475–483.
- [11] A. Bernardini, E. Majorana, P. Puppo, P. Rapagnani, F. Ricci, and G. Testi, "Suspension last stages for the mirrors of the virgo interferometric gravitational wave antenna," *Rev. Sci. Instrum.*, vol. 70, p. 3463.
- [12] F. Acernese *et al.*, "A local control system for the test masses of the virgo gravitational wave detector," *Astroparticle Phys.*, vol. 20, pp. 617–628, 2004.
- [13] H. Tariq *et al.*, "The linear variable differential transformer (LVDT) position sensor for gravitational wave interferometry low-frequency controls," *Nucl. Instrum. Meth. A*, vol. 489, p. 570, 2002.
- [14] S. Braccini *et al.*, "Low noise wide band accelerometer using an inductive displacement sensor," *Rev. Sci. Instrum.*, vol. 66, p. 2672, 1995.
- [15] F. Acernese *et al.*, "First locking of the virgo central area interferometer with suspension hierarchical control," *Astroparticle Phys.*, vol. 20, pp. 629–640, 2004.
- [16] A. Gennai, 2004, Virgo Note VIR-SPE-PIS-4900-120.
- [17] F. Bellachia, D. Boget, B. Mours, and D. Verkindt, The VIRGO Timing System, 1997, Virgo Note VIR-TRE-LAP-5200-103.
- [18] F. Bellachia, D. Boget, B. Mours, and D. Verkindt, Digital Optical Link User's Manual, 1998, Virgo Note VIR-SPE-LAP-5200-105.
- [19] F. Bellachia *et al.*, "A VME basted CCD imaging system for the VIRGO interferometer control," *Nucl. Instrum. Meth. A*, vol. 413, p. 151, 1998.
- [20] F. Acernese *et al.*, "The variable finesse technique," *Class. Quant. Grav.*, vol. 23, pp. S85–S89, 2006.
- [21] F. Carbognani *et al.*, "Automation of the Lock acquisition of the 3 km arm VIRGO interferometer," presented at the 10th ICALPECS Int. Conf. Accelerator Large Expt. Physics Control Systems, Geneva, Oct. 10–14, 2005.
- [22] R. W. P. Drever *et al.*, "Laser phase and frequency stabilization using an optical resonator," *Appl. Phys. B*, vol. 31, p. 97, 1983.
- [23] F. Acernese *et al.*, "The virgo automatic alignment system," *Class. Quant. Grav.*, vol. 23, pp. S91–S101, 2006.
- [24] D. Babusci *et al.*, "Alignment procedure for the VIRGO interferometer: Experimental results from the Frascati prototype," *Phys. Lett. A*, vol. 26, pp. 31–40, 1997.
- [25] W. D. Peterson, *VMEbus Handbook*, 4th ed. Scottsdale, AZ: VITA, 1997.
- [26] M. Barsuglia, Stabilisation en Fréquence du Laser et Contrôle de Cavités Optiques à Miroirs Suspendus Pour le Détecteur Interférométrique D'ondes Gravitationnelles Virgo, LAL 99-25.
- [27] Parallel Sub-System Bus of the IEC 821 VME Bus, The International Organization for Standardization, 1988, ISO/IEC 822.
- [28] RIO2 8062: PowerPC Based RISC I/O Boards, 1998, DOC 8062 UM CES.
- [29] Eugène-Lance, Switzerland, CES—Creative Electronic Systems.
- [30] San Jose, CA, LynuxWorks.
- [31] D. Boget, F. Bellachia, B. Mours, and D. Verkindt, Virgo Note VIR-SPE-LAP-5200-105.
- [32] Datum bc635/637VME and bc350/357VXI Time and Frequency Processor Modules. Irving, CA, Datum, Inc.
- [33] R. Chiche, Transparent Memory Bus Technical and User's Manual, 1999, Virgo Note VIR-SPE-LAL-5500-111.
- [34] F. Cavalier, Le Contrôle Global de Virgo, Mémoire d'habilitation, 2001, LAL 01-69.
- [35] C. Arnault and P. Massart, 1998, Virgo Note VIR-MAN-LAL-5100-112.
- [36] C. Arnault, Virgo Note VIR-MAN-LAL-5600-111.
- [37] IEEE Draft Standard Physical and Environmental Layers for PCI Mezzanine Cards: PMC, IEEE Standard P1386.1draft 2.0.
- [38] PCI Express Base Specification, PCI Special Interest Group, 2005.
- [39] Analog Devices SHARC DSP Microcomputer ADSP-21160N Data Sheet, Analog Devices, Inc., Norwood, MA. [Online]. Available: http://www.analog.com/UploadedFiles/Data_Sheets/ADSP-21160N.pdf
- [40] A. Gennai, 2004, Virgo Note VIR-SPE-PIS-4900-121.